

# Diagnosing New Physics in $b \rightarrow c \tau \nu_\tau$ decays in the light of the recent BaBar result

Alakabha Datta <sup>a,1</sup>, Murugeswaran Duraisamy <sup>a,2</sup>  
and Diptimoy Ghosh <sup>b,3</sup>

*a: Department of Physics and Astronomy, 108 Lewis Hall,  
University of Mississippi, Oxford, MS 38677-1848, USA*

*b: Tata Institute of Fundamental Research  
Homi Bhabha Road, Colaba, Mumbai 400005, India*

(April 21, 2019)

## Abstract

The BaBar Collaboration has recently reported the measurement of the ratio of the branching fractions of  $\bar{B} \rightarrow D(D^*)\tau^-\bar{\nu}_\tau$  to  $\bar{B} \rightarrow D(D^*)\ell^-\bar{\nu}_\ell$  which deviates from the Standard Model prediction by  $2\sigma(2.7\sigma)$ . This deviation goes up to  $3.4\sigma$  level when the two measurements in the  $D$  and  $D^*$  modes are taken together and could indicate new physics. Using an effective Lagrangian for the new physics, we study the implication of these results and calculate other observables that can shed light on the nature of the new physics. We show that the measurements of the forward-backward asymmetries and the  $\tau$  and  $D^*$  polarization fractions can be distinguished among the various couplings of the new physics operators.

## 1 Introduction

The Standard Model (SM) has been extremely successful in furthering the understanding of the various measurements of Branching Ratios (BR) and asymmetries in the quark sector. In the quark flavor sector, the B factories, BABAR and Belle, have produced an enormous quantity of data in the last decade. There is still a lot of data to be analyzed from both experiments. The B factories have firmly established

---

<sup>1</sup>datta@phy.olemiss.edu

<sup>2</sup>duraism@phy.olemiss.edu

<sup>3</sup>diptimoyghosh@theory.tifr.res.in

the CKM mechanism as the leading order contributor to CP violating phenomena in the flavor sector involving quarks. New physics (NP) effects can add to the leading order term producing deviations from the Standard Model (SM) predictions. But even after this incredible success the mechanism of Electroweak Symmetry Breaking (EWSB) and the origin of masses in the SM still remain very poorly understood. In this respect, the second and third generation quarks and leptons are quite special because they are comparatively heavier and are expected to be relatively more sensitive to new physics. As an example, in certain versions of the two Higgs doublet models (2HDM) the couplings of the new Higgs bosons are proportional to the masses and so new physics effects are more pronounced for the heavier generations. Moreover, the constraints on new physics involving, specially the third generation leptons and quarks, are somewhat weaker allowing for larger new physics effects. Interestingly, the branching ratio of  $B \rightarrow \tau \nu_\tau$  shows some tension with the SM predictions [1] and this could indicate NP [2], possibly coming from an extended scalar or gauge sector. There is also a seeming violation of universality in the tau lepton coupling to the W suggested by the Lep II data which could indicate new physics associated with the third generation lepton [3].

If there is NP involving the third generation leptons one can search for it in  $B$  decays such as  $\bar{B} \rightarrow D\tau^-\bar{\nu}_\tau$ ,  $\bar{B} \rightarrow D^*\tau^-\bar{\nu}_\tau$  [4]. The semileptonic decays of B meson to the  $\tau$  lepton is mediated by a  $W$  boson in the SM and it is quite well understood theoretically. In many models of new physics this decay gets contributions from additional states like new vector bosons or new scalar particles. The exclusive decays  $\bar{B} \rightarrow D\tau^-\bar{\nu}_\tau$  and  $\bar{B} \rightarrow D^*\tau^-\bar{\nu}_\tau$  are important places to look for NP because, being three body decays, they offer a host of observables in the angular distributions of the final state particles. The theoretical uncertainties of the SM predictions have gone down significantly in recent years because of the developments in heavy-quark effective theory (HQET). The experimental situation has also improved a lot since the first observation of the decay  $\bar{B} \rightarrow D^*\tau^-\bar{\nu}_\tau$  in 2007 by the Belle Collaboration [5]. After 2007 many improved measurements have been reported by both the BaBar and Belle collaborations and the evidence for the decay  $\bar{B} \rightarrow D\tau^-\bar{\nu}_\tau$  has also been found [6, 7, 8]. Recently, the BaBar collaboration with their full data sample of an integrated luminosity  $426 \text{ fb}^{-1}$  has reported the measurements of the quantities [9]

$$\begin{aligned} R(D) &= \frac{BR(\bar{B} \rightarrow D\tau^-\bar{\nu}_\tau)}{BR(\bar{B} \rightarrow D\ell^-\bar{\nu}_\ell)} = 0.440 \pm 0.058 \pm 0.042, \\ R(D^*) &= \frac{BR(\bar{B} \rightarrow D^*\tau^-\bar{\nu}_\tau)}{BR(\bar{B} \rightarrow D^*\ell^-\bar{\nu}_\ell)} = 0.332 \pm 0.024 \pm 0.018. \end{aligned} \quad (1)$$

The SM predictions for  $R(D)$  and  $R(D^*)$  are [9, 10, 11]

$$\begin{aligned} R(D) &= 0.297 \pm 0.017, \\ R(D^*) &= 0.252 \pm 0.003, \end{aligned} \quad (2)$$

which deviate from the BaBar measurements by  $2\sigma$  and  $2.7\sigma$  respectively. The BaBar collaboration themselves reported a  $3.4\sigma$  deviation from SM when the two measurements of Eq. 1 are taken together.

These deviations could be sign of new physics and already certain models of new physics have been considered to explain the data [12]. In this work, we calculate various observables in  $\bar{B} \rightarrow D\tau^-\bar{\nu}_\tau$  and  $\bar{B} \rightarrow D^*\tau^-\bar{\nu}_\tau$  decays with new physics. We write the most general effective Lagrangian that affect these decays. The Lagrangian contains two quark and two lepton scalar, pseudoscalar, vector, axial vector and tensor operators. Considering subsets of the NP operators at a time, the coefficient of these operators can be fixed from the BaBar measurements and then one can study the effect of these operators on the various observables.

The paper is organized in the following manner. In Sec. 2 we set up our formalism where we introduce the effective Lagrangian for new physics and define the various observables in  $\bar{B} \rightarrow D\tau^-\bar{\nu}_\tau$  and  $\bar{B} \rightarrow D^*\tau^-\bar{\nu}_\tau$  decays. We also present the SM predictions for these observables in that section. In Sec. 3 we present the numerical predictions which include constraints on the new physics couplings as well as predictions for the various observables with new physics. Finally, in Sec. 4 we summarize the results of our analysis.

## 2 Formalism

In the presence of new physics (NP), the effective Hamiltonian for the quark-level transition  $b \rightarrow cl^-\bar{\nu}_l$  can be written in the form [13]

$$\begin{aligned} \mathcal{H}_{eff} = & \frac{4G_F V_{cb}}{\sqrt{2}} \left[ (1 + V_L) [\bar{c}\gamma_\mu P_L b] [\bar{l}\gamma^\mu P_L \nu_l] + V_R [\bar{c}\gamma^\mu P_R b] [\bar{l}\gamma_\mu P_L \nu_l] \right. \\ & \left. + S_L [\bar{c}P_L b] [\bar{l}P_L \nu_l] + S_R [\bar{c}P_R b] [\bar{l}P_L \nu_l] + T_L [\bar{c}\sigma^{\mu\nu} P_L b] [\bar{l}\sigma_{\mu\nu} P_L \nu_l] \right] \quad (3) \end{aligned}$$

where  $G_F = 1.116637 \times 10^{-5} GeV^{-2}$  is the Fermi coupling constant,  $V_{cb}$  is the Cabibbo-Kobayashi-Maskawa (CKM) matrix element.  $P_{L,R} = (1 \mp \gamma_5)/2$  is the projector of negative/positive chirality, and we use  $\sigma_{\mu\nu} = i[\gamma_\mu, \gamma_\nu]/2$ . We have assumed the neutrinos to be always left chiral. Further, we do not assume any relation between  $b \rightarrow ul^-\bar{\nu}_l$  and  $b \rightarrow cl^-\bar{\nu}_l$  transitions and hence do not include constraints from  $B \rightarrow \tau\nu_\tau$ . The SM effective Hamiltonian corresponds to  $V_L = V_R = S_L = S_R = T_L = T_R = 0$ . In this paper we will ignore the tensor interactions. With this simplification we write the effective Lagrangian as

$$\begin{aligned} \mathcal{H}_{eff} = & \frac{G_F V_{cb}}{\sqrt{2}} \left\{ [\bar{c}\gamma_\mu(1 - \gamma_5)b + g_V \bar{c}\gamma_\mu b + g_A \bar{c}\gamma_\mu \gamma_5 b] \bar{l}\gamma^\mu(1 - \gamma_5)\nu_l \right. \\ & \left. + [g_S \bar{c}b + g_P \bar{c}\gamma_5 b] \bar{l}(1 - \gamma_5)\nu_l + h.c. \right\}, \quad (4) \end{aligned}$$

where  $g_{V,A} = V_R \pm V_L$  and  $g_{S,P} = S_R \pm S_L$ .

We will now consider the two cases:

- Case a : In this case we will set  $S_L, S_R = 0$  and assume that the NP affects leptons of only the third generation. This scenario could arise from the exchange of a new charged  $W'$  boson [14].
- Case b : In this case we will set  $V_L, V_R = 0$  and assume that the NP affects only leptons of the third generation. This scenario could arise in models with extended scalar sector [15].

The polar angle differential decay distribution in the momentum transfer squared  $q^2$  for the process  $\bar{B} \rightarrow D^{(*)} l \nu_l$  can be written in the form

$$\frac{d\Gamma}{dq^2 d\cos\theta_l} = \frac{|p_{D^{(*)}}|v_l}{256\pi^3 m_B^2} \sum_{\text{polarization}} |\mathcal{M}(\bar{B} \rightarrow D^{(*)} l \nu_l)|^2, \quad (5)$$

where  $v_l = \sqrt{1 - m_l^2/q^2}$  and the momentum of the  $D^{(*)}$  meson in the B meson rest frame is denoted as  $|p_{D^{(*)}}| = \lambda^{1/2}(m_B^2, m_{D^{(*)}}^2, q^2)/2m_B$  with  $\lambda(a, b, c) = a^2 + b^2 + c^2 - 2(ab + bc + ca)$ .

## 2.1 $\bar{B} \rightarrow D^* \tau^- \bar{\nu}_\tau$ angular distribution

The full  $\bar{B} \rightarrow D^* \tau^- \bar{\nu}_\tau$  angular distribution is given by,

$$\begin{aligned} \frac{d\Gamma^{D^*}}{dq^2 d\cos\theta_l} = & N |p_{D^*}| \left[ 2|\mathcal{A}_0|^2 \sin^2\theta_l + (|\mathcal{A}_\parallel|^2 + |\mathcal{A}_\perp|^2)(1 + \cos\theta_l)^2 - 4\text{Re}[\mathcal{A}_\parallel \mathcal{A}_\perp^*] \cos\theta_l \right. \\ & \left. + \frac{m_\tau^2}{q^2} \left( 2|\mathcal{A}_0 \cos\theta_l - \mathcal{A}_{tP}|^2 + (|\mathcal{A}_\parallel|^2 + |\mathcal{A}_\perp|^2) \sin^2\theta_l \right) \right], \end{aligned} \quad (6)$$

where  $\theta_l$  is the angle between the  $D^*$  meson and the  $\tau$  lepton three-momenta in the  $q^2$  rest frame,  $N = \frac{G_F^2 |V_{cb}|^2 q^2}{256\pi^3 m_B^2} \left(1 - \frac{m_l^2}{q^2}\right)^2$  and the amplitude  $\mathcal{A}_{tP}$  is

$$\mathcal{A}_{tP} = \left( \mathcal{A}_t + \frac{\sqrt{q^2}}{m_\tau} \mathcal{A}_P \right). \quad (7)$$

The differential decay rates for the  $\tau$  helicities,  $\lambda_\tau = \pm 1/2$ , various transversity amplitudes and the form factors are defined in appendix B and D respectively.

The angular distribution allows us to define several observables [10, 11]. The starting point is to obtain the decay rates  $d\Gamma/dq^2$  for the  $\tau$  helicities,  $\lambda_\tau = \pm 1/2$ , after performing integration over  $\cos\theta_l$ ,

$$\begin{aligned}\frac{d\Gamma^{D^*}[\lambda_\tau = -1/2]}{dq^2} &= \frac{8N|p_D|}{3} |\mathcal{A}_T|^2, \\ \frac{d\Gamma^{D^*}[\lambda_\tau = 1/2]}{dq^2} &= \frac{4N|p_D|}{3} \frac{m_\tau^2}{q^2} [|\mathcal{A}_T|^2 + 3|\mathcal{A}_{tP}|^2],\end{aligned}\quad (8)$$

where  $|\mathcal{A}_T|^2 = |\mathcal{A}_0|^2 + |\mathcal{A}_\parallel|^2 + |\mathcal{A}_\perp|^2$ . The summation of these rates give the total differential branching ratio (DBR):

$$\frac{dBr[\bar{B} \rightarrow D^* \tau^- \bar{\nu}_\tau]}{dq^2} = \frac{8N|p_D|\tau_B}{3\hbar} \left[ |\mathcal{A}_T|^2 \left(1 + \frac{m_\tau^2}{2q^2}\right) + \frac{3m_\tau^2}{2q^2} |\mathcal{A}_{tP}|^2 \right]. \quad (9)$$

where  $\tau_B$  is the B meson life-time. Furthermore, one can also explore the  $q^2$  dependent ratio

$$R_{D^*}(q^2) = \frac{dBr[\bar{B} \rightarrow D^* \tau^- \bar{\nu}_\tau]/dq^2}{dBr[\bar{B} \rightarrow D^* \ell^- \bar{\nu}_\ell]/dq^2}, \quad (10)$$

where  $\ell$  denotes the light lepton ( $e, \mu$ ). The ratio  $R_{D^*}(q^2)$  is independent of the form factor  $h_{A_1}(w)$ . The SM predictions of DBR and  $R_{D^*}(q^2)$  for the decay  $\bar{B} \rightarrow D^{0*} \tau^- \bar{\nu}_\tau$  are shown in Fig. 1. The numerical values of  $B \rightarrow D^*$  form factor parameters  $h_{A_1}(1)|V_{cb}|$ ,  $\rho^2$  and  $R_{0,1,2}(1)$  are given in appendix D. In the SM, the DBR for the decay  $\bar{B} \rightarrow D^{0*} \tau^- \bar{\nu}_\tau$  peaks ( $\approx 0.27\% \text{ GeV}^{-2}$ ) at  $q^2 \approx 8 \text{ GeV}^2$ , and the ratio  $R_{D^*}(q^2)$  rises to more than 50% at large  $q^2$ . It is clear from the plot that the uncertainty in  $R_{D^*}(q^2)$  is less than that in the DBR.

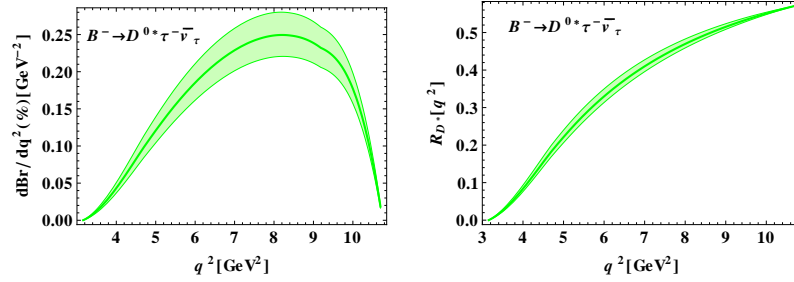


Figure 1: The left (right) panels of the figure show the  $q^2$  dependence of DBR ( $R_{D^*}(q^2)$ ) for the decay  $\bar{B} \rightarrow D^{0*} \tau^- \bar{\nu}_\tau$ . The bands correspond to uncertainties in  $h_{A_1}(1)|V_{cb}|$ ,  $\rho^2$  and  $R_{0,1,2}(1)$ . The errors are added in quadrature.

Next, we define the forward-backward asymmetry (AFB) in the angular distribution by integrating over  $\cos \theta_l$  as

$$[A_{FB}]_{D^*}(q^2) = \frac{(\int_0^1 - \int_{-1}^0) d\cos \theta_l \frac{d\Gamma^{D^*}}{dq^2 d\cos \theta_l}}{\frac{d\Gamma^{D^*}}{dq^2}} = -\frac{3}{2} \frac{\left( Re[\mathcal{A}_\parallel \mathcal{A}_\perp^*] + \frac{m_\tau^2}{q^2} Re[\mathcal{A}_0 \mathcal{A}_{tP}^*] \right)}{|\mathcal{A}_T|^2 \left(1 + \frac{m_\tau^2}{2q^2}\right) + \frac{3m_\tau^2}{2q^2} |\mathcal{A}_{tP}|^2}. \quad (11)$$

The perpendicular transversity amplitude  $\mathcal{A}_\perp$  is proportional to  $\sqrt{w^2 - 1}$  (see appendix B for the details), hence for the light leptons  $[A_{FB}]_{D^*}(q^2)$  vanishes at the end-points due to the kinematics. One can obtain the angular distribution only for the transversely polarized  $D^*$  meson from Eq. (6) by dropping the amplitudes  $\mathcal{A}_0$  and  $\mathcal{A}_{tP}$ . We now define the forward-backward asymmetry for the transversely polarized  $D^*$  meson by integrating over  $\cos \theta_l$  as in Eq. (11) [16]:

$$[A_{FB}^T]_{D^*}(q^2) = -\frac{3}{2} \frac{\text{Re}[\mathcal{A}_\parallel \mathcal{A}_\perp^*]}{(|\mathcal{A}_\parallel|^2 + |\mathcal{A}_\perp|^2) \left(1 + \frac{m_\tau^2}{2q^2}\right)}. \quad (12)$$

Fig. 2 shows the SM predictions for  $[A_{FB}]_{D^*}(q^2)$  and  $[A_{FB}^T]_{D^*}(q^2)$  in the decay  $\bar{B} \rightarrow D^* \tau^- \bar{\nu}_\tau$ .  $[A_{FB}]_{D^*}(q^2)$  is  $\sim 20\%$  and negative at low  $q^2$ , and has a zero crossing at  $q^2 \approx 5.64 \text{ GeV}^2$ . However, the asymmetry  $[A_{FB}^T]_{D^*}(q^2)$  is always positive and large ( $\sim 40\%$ ) at low  $q^2$ .

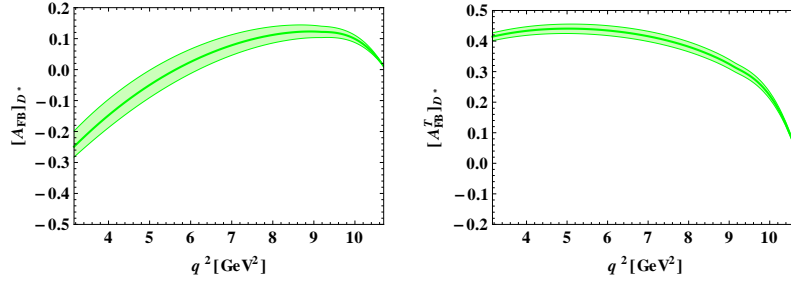


Figure 2: The left (right) panel shows the  $q^2$  dependence of  $[A_{FB}]_{D^*}$  ( $[A_{FB}^T]_{D^*}$ ) for the decay  $\bar{B} \rightarrow D^{0*} \tau^- \bar{\nu}_\tau$ . The bands correspond to uncertainties in  $\rho^2$  and  $R_{0,1,2}(1)$ . The errors are added in quadrature.

We now define the longitudinal and transverse polarization fractions of the  $D^*$  meson from Eq. 9 as

$$\begin{aligned} F_L^{D^*} &= \frac{|\mathcal{A}_0|^2 \left(1 + \frac{m_\tau^2}{2q^2}\right) + \frac{3m_\tau^2}{2q^2} |\mathcal{A}_{tP}|^2}{|\mathcal{A}_T|^2 \left(1 + \frac{m_\tau^2}{2q^2}\right) + \frac{3m_\tau^2}{2q^2} |\mathcal{A}_{tP}|^2}, \\ F_T^{D^*} &= \frac{(|\mathcal{A}_\parallel|^2 + |\mathcal{A}_\perp|^2) \left(1 + \frac{m_\tau^2}{2q^2}\right)}{|\mathcal{A}_T|^2 \left(1 + \frac{m_\tau^2}{2q^2}\right) + \frac{3m_\tau^2}{2q^2} |\mathcal{A}_{tP}|^2}, \end{aligned} \quad (13)$$

where  $F_L^{D^*} + F_T^{D^*} = 1$ . The  $D^*$  polarization fractions can be measured by fitting to the decay distribution in Eq. 6 or from  $D^*$  decays.

Finally, one can also define the longitudinal polarization fraction of the  $\tau$  lepton in the  $q^2$  rest frame as

$$P_L^{*\tau}(q^2) = \frac{\frac{d\Gamma^{D^*}[\lambda_\tau=-1/2]}{dq^2} - \frac{d\Gamma^{D^*}[\lambda_\tau=1/2]}{dq^2}}{\frac{d\Gamma^{D^*}}{dq^2}} = \frac{|\mathcal{A}_T|^2 \left(1 - \frac{m_\tau^2}{2q^2}\right) - \frac{3m_\tau^2}{2q^2} |\mathcal{A}_{tP}|^2}{|\mathcal{A}_T|^2 \left(1 + \frac{m_\tau^2}{2q^2}\right) + \frac{3m_\tau^2}{2q^2} |\mathcal{A}_{tP}|^2}. \quad (14)$$

The  $\tau$  polarization can be measured from the decays of the  $\tau$ .

The polarization fractions are independent of the form factor  $h_{A1}(w)$ . The SM predictions of the longitudinal polarization fractions of  $D^*$  and  $\tau$  are shown in Fig. 3. In the SM,  $F_L^{D^*}(q^2)$  can be as large as 0.75 at low  $q^2$ , and it decreases to about 0.4 at high  $q^2$ . On the other hand,  $P_L^{*\tau}(q^2)$  is about -0.18 at very low  $q^2$  and has a zero-crossing at  $q^2 \approx 3.64 \text{ GeV}^2$  and increases to about 0.7 at high  $q^2$ .

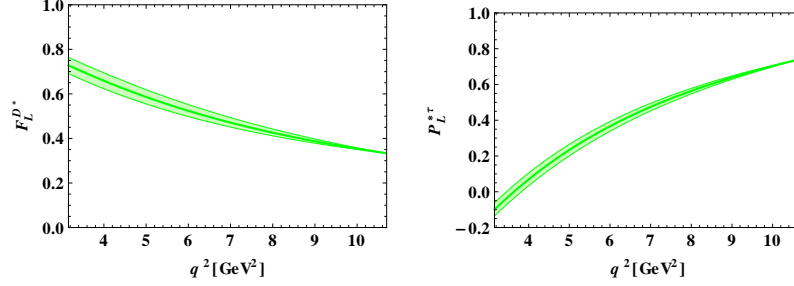


Figure 3: The left (right) panel shows the  $q^2$  dependence of  $F_L^{D^*}$  ( $P_L^{*\tau}$ ) for the decay  $\bar{B} \rightarrow D^{0*}\tau^-\bar{\nu}_\tau$ . The bands correspond to uncertainties in  $\rho^2$  and  $R_{0,1,2}(1)$ . The errors are added in quadrature.

## 2.2 $\bar{B} \rightarrow D\tau^-\bar{\nu}_\tau$ angular distribution

The full  $\bar{B} \rightarrow D\tau^-\bar{\nu}_\tau$  angular distribution can be written as,

$$\frac{d\Gamma^D}{dq^2 d\cos\theta_l} = N|p_D| \left[ 2|H_0|^2 \sin^2\theta_l + 2\frac{m_\tau^2}{q^2}(H_0 \cos\theta_l - H_{tS})^2 \right], \quad (15)$$

where

$$H_{tS} = \left( H_t - \frac{\sqrt{q^2}}{m_\tau} H_S \right). \quad (16)$$

The differential decay rates for the  $\tau$  helicities,  $\lambda_\tau = \pm 1/2$ , and helicity amplitudes  $H_0$  are defined in appendix C.

As in the previous section, we can define several observables using the  $\bar{B} \rightarrow D\tau^-\bar{\nu}_\tau$  angular distribution [11]. The starting point is to obtain the decay rates  $d\Gamma/dq^2$  for the  $\tau$  helicities,  $\lambda_\tau = \pm 1/2$ . After performing integration over  $\cos\theta_l$ , one can obtain:

$$\begin{aligned} \frac{d\Gamma^D[\lambda_\tau = -1/2]}{dq^2} &= \frac{8}{3}N|p_D||H_0|^2, \\ \frac{d\Gamma^D[\lambda_\tau = 1/2]}{dq^2} &= \frac{4}{3}N|p_D|\frac{m_\tau^2}{q^2}(|H_0|^2 + 3|H_{tS}|^2), \end{aligned} \quad (17)$$

and the summation of these differential decay rates give the DBR

$$\frac{dBr[\bar{B} \rightarrow D\tau^-\bar{\nu}_\tau]}{dq^2} = \frac{8N|p_D|\tau_B}{3\hbar} \left[ |H_0|^2 \left(1 + \frac{m_\tau^2}{2q^2}\right) + \frac{3m_\tau^2}{2q^2} |H_{tS}|^2 \right]. \quad (18)$$

As in the previous section, one can also explore the  $q^2$  dependent ratio

$$R_D(q^2) = \frac{dBr[\bar{B} \rightarrow D\tau^-\bar{\nu}_\tau]/dq^2}{dBr[\bar{B} \rightarrow D\ell^-\bar{\nu}_\ell]/dq^2}. \quad (19)$$

The ratio  $R_D(q^2)$  is independent of the form factors. The SM predictions of DBR and  $R_D(q^2)$  for the decay  $\bar{B} \rightarrow D^0\tau^-\bar{\nu}_\tau$  are shown in Fig. 4. The numerical values of the free parameters in the  $B \rightarrow D$  form factors are given in appendix C. In the SM, the DBR for the decay  $\bar{B} \rightarrow D^0\tau^-\bar{\nu}_\tau$  peaks ( $\approx 0.14\%$   $\text{GeV}^{-2}$ ) at  $q^2 \approx 7 \text{ GeV}^2$ , while  $R_D(q^2)$  shows almost a linear behavior with  $q^2$ .

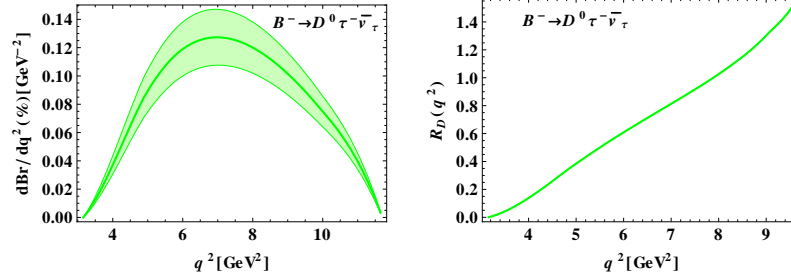


Figure 4: The left (right) panel shows the  $q^2$  dependence of DBR (  $R_D(q^2)$  ) for the decay  $\bar{B} \rightarrow D^0\tau^-\bar{\nu}_\tau$ . The bands correspond to uncertainties in  $V_1(1)|V_{cb}|$ ,  $\rho^2$  and  $\rho_1^2$ . The errors are added in quadrature.

Next, we define the forward-backward asymmetry in the angular distribution by integrating over  $\cos \theta_l$  as

$$[A_{FB}]_D(q^2) = \frac{(\int_{-1}^0 - \int_0^1) d\cos \theta_l \frac{d\Gamma^D}{dq^2 d\cos \theta_l}}{\frac{d\Gamma^D}{dq^2}} = \frac{3m_\tau^2}{2q^2} \frac{\text{Re}[H_0 H_{tS}^*]}{|H_0|^2 \left(1 + \frac{m_\tau^2}{2q^2}\right) + \frac{3m_\tau^2}{2q^2} |H_{tS}|^2}. \quad (20)$$

Finally, we define the longitudinal polarization fraction of  $\tau$  in the  $q^2$  rest frame as

$$P_L^\tau(q^2) = \frac{\frac{d\Gamma^D[\lambda_\tau=1/2]}{dq^2} - \frac{d\Gamma^D[\lambda_\tau=-1/2]}{dq^2}}{\frac{d\Gamma^D}{dq^2}} = \frac{|H_0|^2 \left(\frac{m_\tau^2}{2q^2} - 1\right) + \frac{3m_\tau^2}{2q^2} |H_{tS}|^2}{|H_0|^2 \left(1 + \frac{m_\tau^2}{2q^2}\right) + \frac{3m_\tau^2}{2q^2} |H_{tS}|^2}. \quad (21)$$

The  $\tau$  polarization can be measured from the decays of the  $\tau$ .

Fig. 5 shows the SM predictions for  $[A_{FB}]_D(q^2)$  and  $P_L^\tau(q^2)$  for the decay  $\bar{B} \rightarrow D^0\tau^-\bar{\nu}_\tau$ . The forward-backward asymmetry,  $[A_{FB}]_D(q^2)$ , is about  $\sim 50\%$  at low  $q^2$  and decreases with increasing  $q^2$ . The  $\tau$  polarization,  $P_L^\tau$ , is about 0.4 at low  $q^2$  and starts to increase after  $q^2 = 8 \text{ GeV}^2$ .

In the next section we shall study the effect of the new physics couplings  $V_{L,R}$  and  $S_{L,R}$  on the above observables.



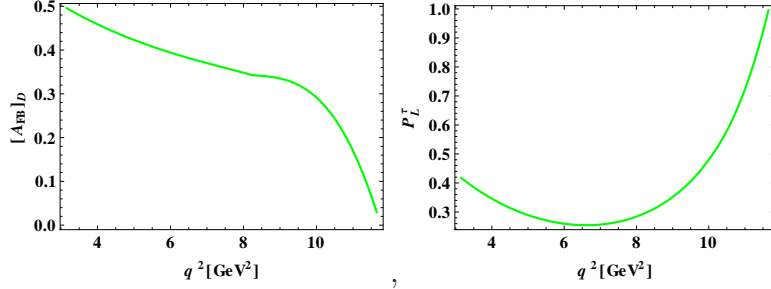


Figure 5: The left (right) panel shows the  $q^2$  dependence of  $[A_{FB}]_D$  ( $P_L^\tau$ ) for the decay  $\bar{B} \rightarrow D^0 \tau^- \bar{\nu}_\tau$ .

### 3 Numerical analysis with NP

In the numerical analysis, as indicated earlier, we consider two cases to study the new physics effects on DBR, the ratios  $R_{D(D^*)}(q^2)$ , the forward-backward asymmetries, and polarization fractions. In the first case we consider only vector/axial-vector NP couplings while in the second case we consider only scalar/pseudoscalar NP couplings. The numerical values of  $B \rightarrow D$  and  $B \rightarrow D^*$  form factors in the heavy quark effective theory framework are summarized in appendix D. A detail discussion of these form factor can be found in [17].

In our numerical analysis, we constrain both complex/real NP couplings  $V_{L,R}$  and  $S_{L,R}$  using the measured  $R(D)$  and  $R(D^*)$  in Eq. (1) at 95% C.L. We also vary the free parameters in the form factors discussed in appendix D within their error bars. All the other numerical values are taken from [18] and [19]. The allowed ranges for NP couplings are then used for predicting the allowed ranges for the observables discussed earlier.

#### 3.1 $\bar{B} \rightarrow D^{0*} \tau^- \bar{\nu}_\tau$

##### 3.1.1 Pure $V_L$ and $V_R$ couplings present

The combination of the couplings  $g_V = V_R + V_L$  appears in both  $R(D)$  and  $R(D^*)$ , while  $g_A = V_R - V_L$  appears only in  $R(D^*)$ .  $V_R$  and  $V_L$  receive constraints from both  $R(D)$  and  $R(D^*)$ . If new physics is established in both  $R(D)$  and  $R(D^*)$  then the case of pure  $g_A$  coupling is ruled out. The constraints on the complex couplings  $g_V$  and  $g_A$  are shown in the colored region of Fig. 6 (left) and (center). Fig. (6)(right) shows the constraints on the real couplings  $V_L$  and  $V_R$ . The real couplings are severely constraints by the recent  $R(D)$  and  $R(D^*)$  measurements. The plot indicates that the data prefers either pure vector or pure axial vector couplings. Henceforth we will consider all three cases which include pure  $g_V$  and  $g_A$  complex couplings and real ( $V_L, V_R$ ) couplings..

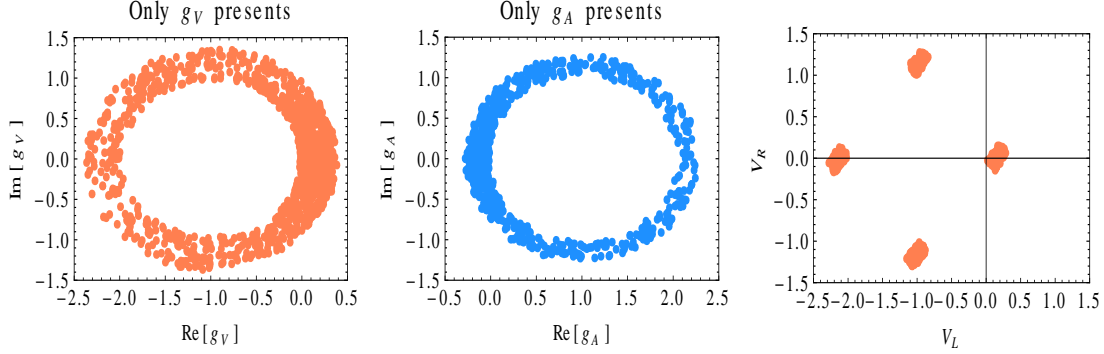


Figure 6: The constraints on the complex coupling  $g_V = V_R + V_L$ ,  $g_A = V_R - V_L$  and the real  $(V_R, V_L)$  couplings at 95% C.L.

### 3.1.2 Only $g_V$ coupling present

In this section we consider only vector coupling  $g_V = V_R + V_L$ . The NP vector coupling  $g_V$  appears only in the amplitude  $\mathcal{A}_\perp$  and except for the forward-backward asymmetries, it does not significantly affect any other observables discussed earlier for the decay  $\bar{B} \rightarrow D^{0*} \tau^- \bar{\nu}_\tau$ . One can see from Fig. 7 that the coupling  $g_V$  can

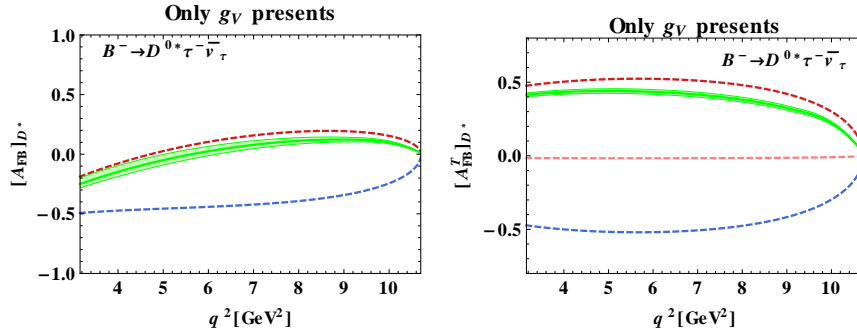


Figure 7: The left (right) panel shows the  $q^2$  dependence of  $[A_{FB}]_{D^*}$  ( $[A_{FB}^T]_{D^*}$ ) for the decay  $\bar{B} \rightarrow D^{0*} \tau^- \bar{\nu}_\tau$ . The dashed lines show predictions for some representative values of  $g_V$ . For example blue lines correspond to  $g_V = 2.34e^{-i3.08}$ .

enhance the magnitude of  $[A_{FB}]_{D^*}$  up to 50% at low  $q^2$  and it can have different zero-crossing point than the SM. In the SM, no zero-crossing is allowed for  $[A_{FB}^T]_{D^*}$ , however in the presence of  $g_V$ ,  $[A_{FB}^T]_{D^*}$  may have zero-crossing. Also,  $[A_{FB}^T]_{D^*}$  can reach up to 50% at low  $q^2$ , and it can have either positive or negative sign.

### 3.1.3 Only $g_A$ coupling present

In this section, we consider only pure axial vector coupling  $g_V = V_R - V_L$ . In this case, except  $\mathcal{A}_\perp$  all other amplitudes depend on the new axial-vector coupling  $g_A$  while the amplitude  $\mathcal{A}_P$  is zero. Thus, the coupling  $g_A$  does not significantly change the values for the polarization fractions of the  $D^*$  meson and the  $\tau$  lepton from their SM predictions. In Fig. 8 we show the DBR and  $R_{D^*}(q^2)$  in the presence of  $g_A$ . The coupling  $g_A$  can enhance DBR up to  $0.4\% \text{ GeV}^{-2}$  at  $q^2 \approx 8.5 \text{ GeV}^2$ , and  $R_{D^*}(q^2)$  can be as high as about 0.9 at high  $q^2$ . As shown in Fig. 9, the coupling  $g_A$  can enhance

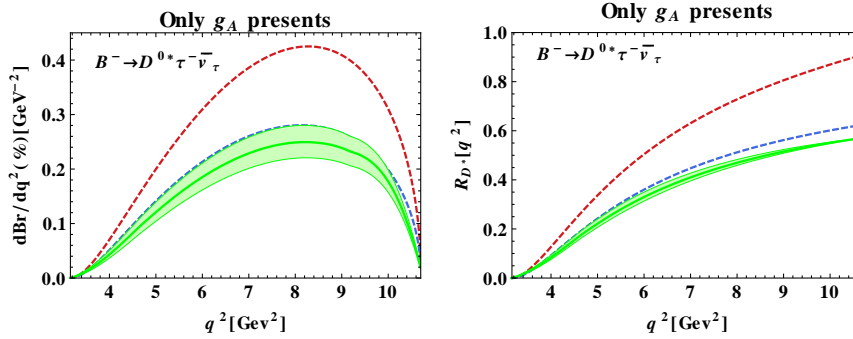


Figure 8: The left (right) panel shows the  $q^2$  dependence of DBR ( $R_{D^*}(q^2)$ ) for the decay  $\bar{B} \rightarrow D^{0*} \tau^- \bar{\nu}_\tau$ . The dashed lines show predictions for some representative values of  $g_A$ . For example, the red lines correspond to  $g_A = 0.31e^{-i2.62}$ .

the magnitude of  $[A_{FB}]_{D^*}$  to about 50% at low  $q^2$  and it can now have different zero-crossing point than the SM. In the SM, no zero-crossing is allowed for  $[A_{FB}^T]_{D^*}$ , however in the presence of  $g_A$ ,  $[A_{FB}^T]_{D^*}$  may have zero-crossing. Also,  $[A_{FB}^T]_{D^*}$  can take either positive or negative sign. The results are similar to the case where only  $g_V$  coupling is present.

### 3.1.4 Both $V_{L,R}$ coupling are present and are real

Finally, we consider the case where both  $V_{L,R}$  coupling are present and are real. In Fig. 10 we show the DBR and  $R_{D^*}(q^2)$  in the presence of both  $V_L$  and  $V_R$  real couplings. These couplings can enhance the DBR upto  $0.4\% \text{ GeV}^{-2}$  at  $q^2 \approx 8.5 \text{ GeV}^2$ , and  $R_{D^*}(q^2)$  can be increased to about 0.9 at high  $q^2$ .

One can see from Fig. 11, the couplings  $V_L$  and  $V_R$  can negatively enhance  $[A_{FB}]_{D^*}$  upto 50% at low  $q^2$  and it can have a different zero-crossing than the SM. In the SM, no zero-crossing is allowed for  $[A_{FB}^T]_{D^*}$ , however in the presence of these new couplings  $[A_{FB}^T]_{D^*}$  may have zero-crossing. Also,  $[A_{FB}^T]_{D^*}$  can reach upto 50% at low  $q^2$ , and it can take either positive or negative values.

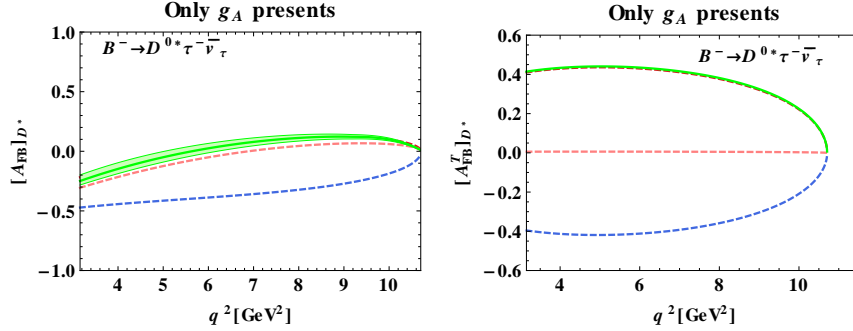


Figure 9: The left (right) panels of the figure show the  $q^2$  dependence of  $[A_{FB}]_{D^*}$  ( $[A_{FB}^T]_{D^*}$ ) for the decay  $\bar{B} \rightarrow D^{0*} \tau^- \bar{\nu}_\tau$ . The dashed lines show predictions for some representative values of  $g_A$ . For example the blue lines correspond to  $g_A = 2.34e^{-i3.08}$ .

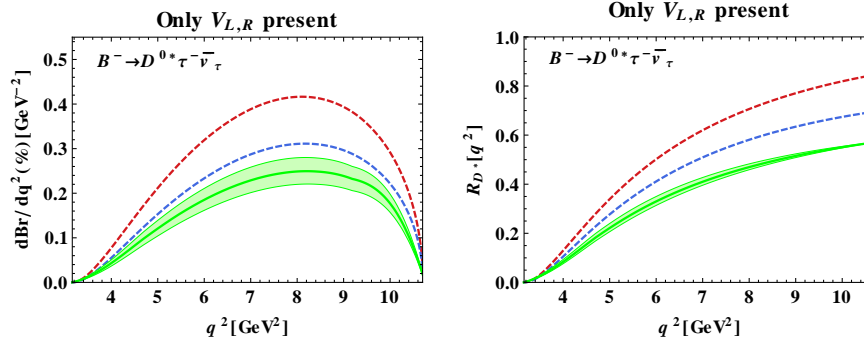


Figure 10: The left (right) panel shows the  $q^2$  dependence of DBR ( $R_{D^*}(q^2)$ ) for the decay  $\bar{B} \rightarrow D^{0*} \tau^- \bar{\nu}_\tau$ . The dashed lines show predictions for some representative values of  $(V_L, V_R)$ . For example the red lines in correspond to  $(V_L, V_R) = (-0.97, 1.24)$ .

The polarization fractions of the  $D^*$  meson are almost independent of the new couplings  $V_L$  and  $V_R$ . The tau lepton polarization fraction too does not depend on  $V_L$  and  $V_R$ .

### 3.1.5 Pure $S_L$ and $S_R$ couplings present

In this section we consider the scalar and pseudo-scalar couplings  $S_{L,R}$ . The combination of the couplings  $S_R + S_L$  appears only in  $R(D)$ , while  $S_R - S_L$  appears only in  $R(D^*)$ . If new physics is established in both  $R(D)$  and  $R(D^*)$  then the cases of pure  $S_R \pm S_L$  couplings are ruled out.

Hence,  $S_R$  and  $S_L$  get constrained from both  $R(D)$  and  $R(D^*)$ . The constraints on the complex couplings  $S_R + S_L$  and  $S_R - S_L$  are shown in Fig. 12 (left and

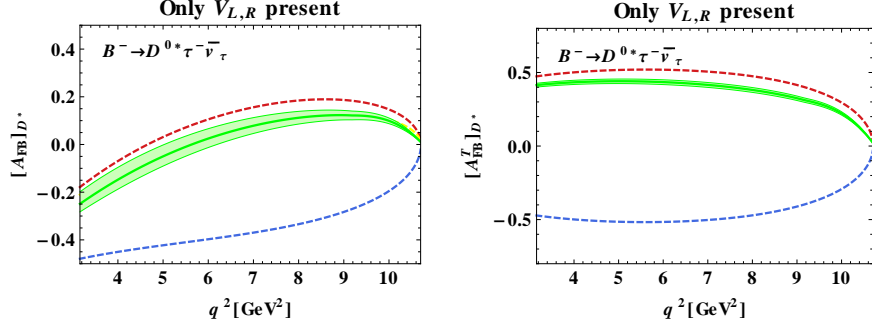


Figure 11: The left (right) panel shows the  $q^2$  dependence of  $[A_{FB}]_{D^*}$  ( $[A_{FB}^T]_{D^*}$ ) for the decay  $\bar{B} \rightarrow D^{0*} \tau^- \bar{\nu}_\tau$ . The dashed lines show predictions for some representative values of  $g_V$ . For example the blue lines correspond to  $(V_L, V_R) = (-1.02, 1.08)$  in the left panel and  $(V_L, V_R) = (-0.85, 1.21)$  in the right panel.

middle). Fig. 12(right) shows the constraints on the real couplings  $S_L$  and  $S_R$ . The real couplings are severely constrained by the recent  $R(D)$  and  $R(D^*)$  measurements though the constraints are relatively weaker than those in the  $(V_L, V_R)$  case. To simplify our discussion we will take  $S_{L,R}$  to be real.

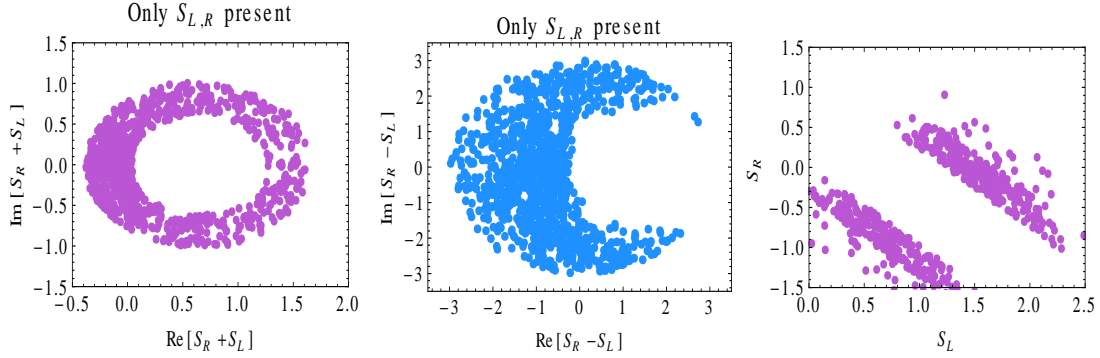


Figure 12: The constraints on the couplings for complex  $(S_R + S_L)$  (left), complex  $(S_R - S_L)$  (center), and real  $S_L$  and  $S_R$  (right) at 95% C.L. .

The combination of couplings  $S_R - S_L$  appears only in the amplitude  $\mathcal{A}_P$ . In Fig. 13 we show the DBR and  $R_{D^*}(q^2)$  in the presence of  $S_L$  and  $S_R$  couplings. These couplings can enhance the DBR up to  $0.4\% \text{ GeV}^{-2}$  at  $q^2 \approx 7.5 \text{ GeV}^2$ . Note that the peak of the DBR is shifted to low  $q^2$  direction relative to the SM. The ratio,  $R_{D^*}(q^2)$ , can take the value of about 0.7 at  $q^2 \approx 7.5 \text{ GeV}^2$ .

The transverse forward-backward asymmetry  $[A_{FB}^T]_{D^*}$  is not sensitive to the  $S_L$  and  $S_R$  couplings. In Fig. 14 we show the effects of  $S_L$  and  $S_R$  on  $[A_{FB}]_{D^*}$ , the polarization fractions  $F_L^{D^*}(q^2)$  and  $P_L^{*\tau}(q^2)$ . These couplings can positively or

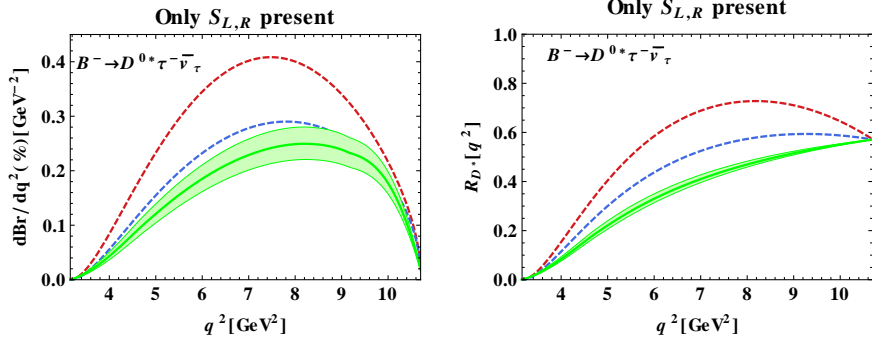


Figure 13: The left (right) panel shows the  $q^2$  dependence of DBR ( $R_{D^*}(q^2)$ ) for the decay  $\bar{B} \rightarrow D^{0*} \tau^- \bar{\nu}_\tau$ . The dashed lines show predictions for some representative values of  $S_L$  and  $S_R$ . For example the red lines correspond to  $(S_L, S_R) = (1.11, -1.30)$ .

negatively enhance  $[A_{FB}]_{D^*}$  to about 30% at low  $q^2$  and there can be different zero-crossing than the SM. Unlike the  $V_L$  and  $V_R$  case, the polarization fractions are sensitive to the  $S_L$  and  $S_R$  couplings. Due to the  $S_L$  and  $S_R$  couplings,  $F_L^{D^*}(q^2)$  can be as large as 0.85 at low  $q^2$ , and it decreases to the SM value at high  $q^2$ . The polarization fraction  $P_L^{*\tau}(q^2)$  can be as large as 0.5 and negative at very low  $q^2$  and can have different zero-crossing than the SM. It increases to the SM value at high  $q^2$ .

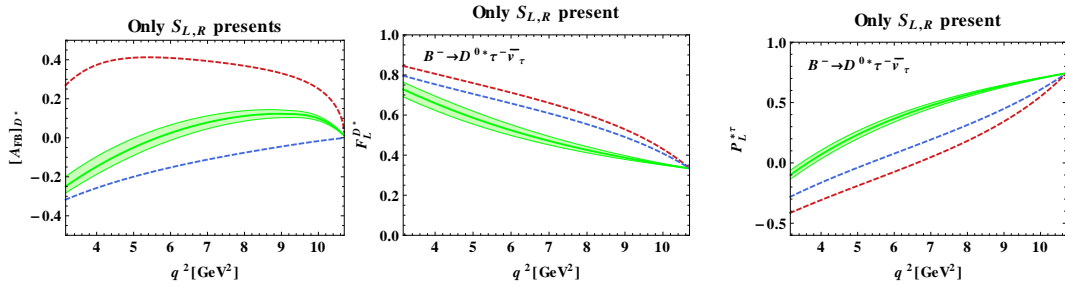


Figure 14: The left (center) and right panel shows the  $q^2$  dependence of  $[A_{FB}]_{D^*}$  ( $F_L^{D^*}$ ) and  $P_L^{*\tau}$  for the decay  $\bar{B} \rightarrow D^{0*} \tau^- \bar{\nu}_\tau$ . The dashed lines show predictions for some representative values of the new couplings  $S_L$  and  $S_R$ . For example the red lines corresponds to  $(S_L, S_R) = (-1.93, 1.73)$  in the left panel,  $(S_L, S_R) = (0.80, -0.9)$  in the middle panel and  $(S_L, S_R) = (0.61, -0.98)$  in the right panel.

### 3.2 $\bar{B} \rightarrow D^0 \tau^- \bar{\nu}_\tau$

#### 3.2.1 Only $g_V$ coupling present

We now consider predictions for the various observables in  $\bar{B} \rightarrow D^0 \tau^- \bar{\nu}_\tau$ . The axial vector coupling  $g_A$  does not contribute in this case and hence we consider only the coupling  $g_V$ . Note that, the forward-backward asymmetry and the  $\tau$  polarization fraction are independent of the coupling  $g_V$ .

In the presence of  $g_V$ , the  $q^2$  dependence of DBR and  $R_D(q^2)$  for the decay  $\bar{B} \rightarrow D^0 \tau^- \bar{\nu}_\tau$  are shown in Fig. 15. The DBR can increase upto 0.25% at  $q^2 \approx 7 \text{ GeV}^2$ . The ratio  $R_D(q^2)$  is proportional to  $(1 + g_V)^2$  and increases with  $q^2$ .

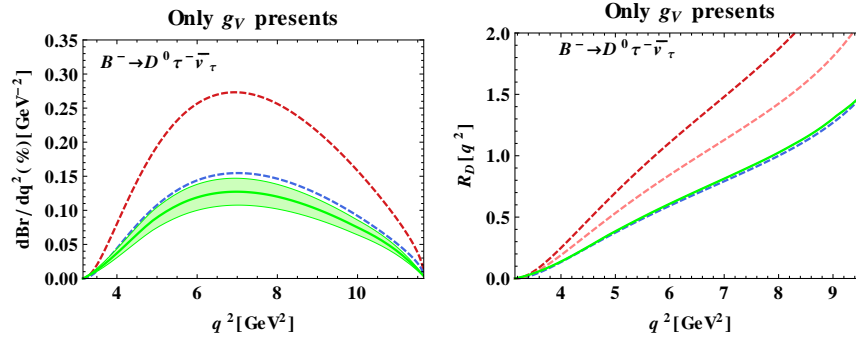


Figure 15: The left (right) panel shows the  $q^2$  dependence of DBR ( $R_D(q^2)$ ) for the decay  $\bar{B} \rightarrow D^0 \tau^- \bar{\nu}_\tau$ . The dashed lines show predictions for some representative values of  $g_V$ . For example the red lines correspond to  $g_V = 0.68e^{i1.27}$  in the left panel and  $g_V = 0.62e^{i1.20}$  in the right panel.

Now we consider  $V_{L,R}$  real and independent. The  $q^2$  dependence of DBR and  $R_D(q^2)$  for the decay  $\bar{B} \rightarrow D^0 \tau^- \bar{\nu}_\tau$  are shown in Fig. 16. The predicted deviations from the SM are similar to the case with pure  $g_V$  coupling.

#### 3.2.2 Pure $S_L$ and $S_R$ couplings present

Finally, we consider the effect of  $S_{L,R}$ , taken to be real, on the observables in  $\bar{B} \rightarrow D^0 \tau^- \bar{\nu}_\tau$ . The allowed ranges for the real  $S_L$  and  $S_R$  couplings are shown as the colored region of Fig. 12(right panel).

In Fig. 17 we show the effect of  $S_L$  and  $S_R$  couplings on the DBR and  $R_D(q^2)$  in the decay  $\bar{B} \rightarrow D^0 \tau^- \bar{\nu}_\tau$ . The DBR increases up to  $0.25\% \text{ GeV}^{-2}$  at  $q^2 \approx 9.5 \text{ GeV}^2$ . Note that the peak of the distribution in the DBR can be shifted towards high  $q^2$  relative to the SM. The deviation in the ratio  $R_D(q^2)$  increases with  $q^2$ .

Unlike the  $V_{L,R}$  case, the forward-backward asymmetry and  $\tau$ -polarization fraction in the decay  $\bar{B} \rightarrow D^0 \tau^- \bar{\nu}_\tau$  are very sensitive to the  $S_L$  and  $S_R$  couplings as shown in Fig. 18. In this case,  $[A_{FB}]_D$  can be either positive or negative, and

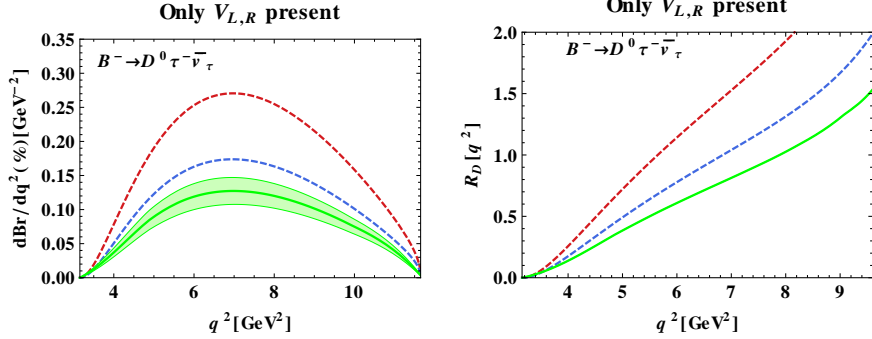


Figure 16: The left (right) panel shows the  $q^2$  dependence of DBR ( $R_D(q^2)$ ) for the decay  $\bar{B} \rightarrow D^0 \tau^- \bar{\nu}_\tau$ . The dashed lines show predictions for some representative values of new couplings  $V_L$  and  $V_R$ . For example the red lines correspond to  $(V_L, V_R) = (-1.09, -1.28)$ .

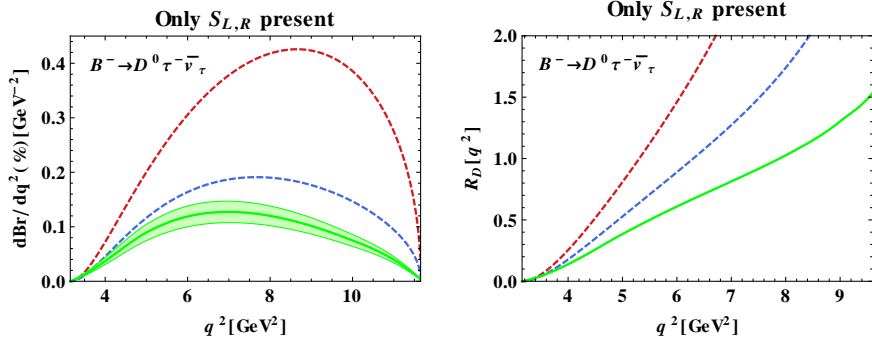


Figure 17: The left (right) panels of the figure show the  $q^2$  dependence of DBR ( $R_D(q^2)$ ) for the decay  $\bar{B} \rightarrow D^0 \tau^- \bar{\nu}_\tau$ . The dashed lines show predictions for some representative values of new couplings  $S_L$  and  $S_R$ . For example the red lines correspond to  $(S_L, S_R) = (0.51, -1.29)$ .

may have zero-crossing. In the SM, there is no zero-crossing for  $[A_{FB}]_D$ . The  $\tau$ -polarization fraction can be negatively enhanced to more than 40% at low  $q^2$  and may have the zero-crossing.

## 4 Summary

In summary, we have considered new physics explanation of the recent measurements in  $\bar{B} \rightarrow D^{0*} \tau^- \bar{\nu}_\tau$  and  $\bar{B} \rightarrow D \tau^- \bar{\nu}_\tau$  decays by the BaBar collaboration. We considered an effective Lagrangian description of the new physics with four-fermi operators with vector/axial vector and scalar/pseudoscalar couplings. We considered two cases, in the first case we considered only V/A couplings and in the second



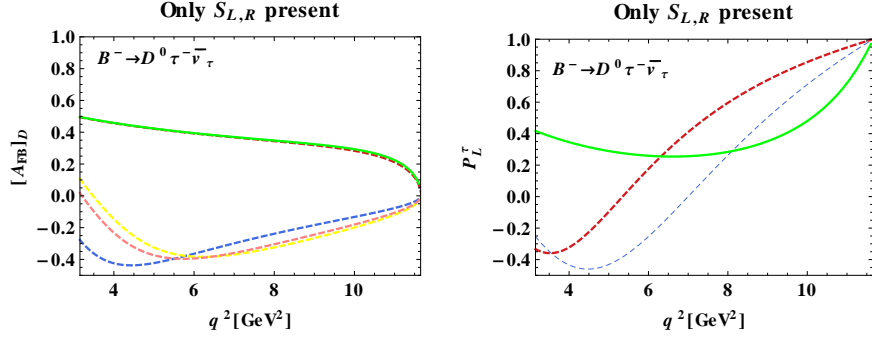


Figure 18: The left (right) panel shows the  $q^2$  dependence of  $[A_{FB}]_D$  ( $P_L^\tau$ ) for the decay  $\bar{B} \rightarrow D^0 \tau^- \bar{\nu}_\tau$ . The dashed lines show predictions for some representative values of new couplings  $S_L$  and  $S_R$ . For example the red lines correspond to  $(S_L, S_R) = (2.11, -0.04)$  in the left panel and  $(S_L, S_R) = (1.42, 0.21)$  in the right panel.

case we considered only S/P couplings. We found that the measurements in the decay  $\bar{B} \rightarrow D^{0*} \tau^- \bar{\nu}_\tau$  strongly constrain the new physics couplings to be only pure vector or pure axial vector. Assuming a pure vector and pure axial vector complex couplings we calculated the differential branching ratios, the ratio  $R_{D^*}(q^2)$ , the forward-backward asymmetries and the polarization fractions of the tau and the  $D^*$  meson. We found that the pure complex vector couplings  $g_V$  only affects the forward-backward asymmetries. The complex axial vector couplings, on the other hand, affects the DBR,  $R_{D^*}(q^2)$  as well as the forward-backward asymmetries. The polarization fractions are not affected in presence of the  $g_{V,A}$  couplings. When we considered real scalar couplings  $S_{L,R}$ , we found that all observables except the transverse forward-backward asymmetry for the  $D^*$ ,  $[A_{FB}^T]_{D^*}$  were affected. Moving on to the decay  $\bar{B} \rightarrow D^0 \tau^- \bar{\nu}_\tau$  we found that the axial vector new physics coupling do not contribute to this decay. In the case of the vector coupling  $g_V$ , the forward-backward asymmetry and the tau polarization fraction were not affected though the DBR and the ratio  $R_D(q^2)$  were affected. In the presence of the scalar couplings  $S_{L,R}$ , not only the DBR and the ratio  $R_D(q^2)$  were affected but the forward-backward asymmetry and the tau polarization fraction were also affected and were found to be very sensitive to the scalar couplings. The fact that different new physics couplings have different effects on the observables demonstrated that by measuring the various observables it is possible to distinguish different models of new physics. Finally, if new physics is established in both  $R(D)$  and  $R(D^*)$  then the cases of pure  $g_A = V_R - V_L$  and pure  $S_R - S_L$  couplings are ruled out as they contribute to only  $R(D^*)$  and the pure  $S_R + S_L$  is ruled out as it contributes to only  $R(D)$ .

## Acknowledgements

We thank Gilad Perez, M. Papucci, M. Gonzalez-Alonso and J. F. Kamenik for useful discussion and comments. DG thanks Amol Dighe for discussion and encouragement. This work was financially supported by the US-Egypt Joint Board on Scientific and Technological Co-operation award (Project ID: 1855) administered by the US Department of Agriculture and in part by the National Science Foundation under Grant No. NSF PHY-1068052. AD thanks the hospitality of the CERN theory group where the work was completed.

## Appendix

### A Kinematics

The matrix element square for the decay  $\bar{B} \rightarrow D^{(*)} l \nu_l$  can be factorized into leptonic ( $L_{\mu\nu}$ ) and hadronic ( $H_{\mu\nu}$ ) tensors as

$$|\mathcal{M}(\bar{B} \rightarrow D^{(*)} l \nu_l)|^2 = |\langle D^{(*)} l \nu | \mathcal{L}_{eff} | \bar{B} \rangle|^2 = L_{\mu\nu} H^{\mu\nu}. \quad (22)$$

The polar angle  $\cos \theta_l$  dependence of the leptonic and hadronic tensors  $L_{\mu\nu} H^{\mu\nu}$  can be evaluated using the completeness relation for the polarization four-vectors  $\bar{\epsilon}(m = 0, \pm, t)$  [20, 21]:

$$\sum_{m, m'=0, \pm, t} \bar{\epsilon}^\mu(m) \bar{\epsilon}^{*\nu}(m') g_{mm'} = g^{\mu\nu}, \quad (23)$$

where the tensor  $g_{mm'} = \text{diag}(+, -, -, -)$ . The matrix element square reduces to

$$|\mathcal{M}(\bar{B} \rightarrow D^{(*)} l \nu_l)|^2 = \sum_{m, m', n, n'} L(m, n) H(m', n') g_{mm'} g_{nn'}, \quad (24)$$

where  $L(m, n) = L^{\mu\nu} \bar{\epsilon}_\mu(m) \bar{\epsilon}_\nu^*(n)$  and  $H(m, n) = H^{\mu\nu} \bar{\epsilon}_\mu^*(m) \bar{\epsilon}_\nu(n)$ . The advantage of Eq.24 is that  $L(m, n)$  and  $H(m', n')$  are Lorentz invariant and so one can evaluate them in different Lorentz frames [21]. The leptonic tensor  $L[m, n]$  will be evaluated in the  $l - \nu_l$  center-of-mass (c.m.) frame ( $q^2$  rest frame), whereas the hadronic tensor  $H[m, n]$  in the B rest frame.

In  $B$  rest frame, we choose the helicity basis  $\bar{\epsilon}$

$$\begin{aligned} \bar{\epsilon}(0) &= \frac{1}{\sqrt{q^2}}(|p_{D^{(*)}}|, 0, 0, -q_0), & \bar{\epsilon}(\pm) &= \pm \frac{1}{\sqrt{q^2}}(0, \pm 1, -i, 0), \\ \bar{\epsilon}(t) &= \frac{1}{\sqrt{q^2}}(q_0, 0, 0, |p_{D^{(*)}}|), \end{aligned} \quad (25)$$

where  $q_0 = (m_B^2 - m_{D^*}^2 + q^2)/2m_B$  and  $|p_{D^*}| = \lambda^{1/2}(m_B^2, m_{D^*}^2, q^2)/2m_B$ . In this frame, the B and  $D^*$  mesons four-momenta  $p_B$  and  $p_{D^*}$  are

$$p_B = (m_B, 0, 0, 0), \quad p_{D^*} = (E_{D^*}, 0, 0, |p_{D^*}|), \quad (26)$$

where  $E_{D^*} = (m_B^2 + m_{D^*}^2 - q^2)/2m_B$ . The momentum transfer  $q$  is  $q = p_B - p_{D^*}$ . Further, one chooses the polarization vector of the  $D^*$  meson as

$$\bar{\epsilon}(0) = \frac{1}{m_{D^*}}(|p_{D^*}|, 0, 0, E_{D^*}), \quad \bar{\epsilon}(\pm) = \mp \frac{1}{2}(0, 1, \pm i, 0). \quad (27)$$

The leptonic tensor  $L[m, n]$  will be evaluated in the  $q^2$  rest frame. In this frame, we choose the transverse components of helicity basis  $\bar{\epsilon}$  to remain the same and other two components are taken as

$$\bar{\epsilon}(0) = (0, 0, 0, -1), \quad \bar{\epsilon}(t) = (1, 0, 0, 0). \quad (28)$$

Let  $\theta_l$  be the angle between the  $D^*$  meson and the  $\tau$  lepton three-momenta in the  $q^2$  rest frame. We define the momenta of the lepton and anti-neutrino pair as

$$\begin{aligned} p_l^\mu &= (E_l, pl \sin \theta_l, 0, -pl \cos \theta_l), \\ p_\nu^\mu &= (p_l, -pl \sin \theta_l, 0, pl \cos \theta_l), \end{aligned} \quad (29)$$

where the lepton energy  $E_l = (q^2 + m_l^2)/2\sqrt{q^2}$  and magnitude of its three-momenta is  $p_l = (q^2 - m_l^2)/2\sqrt{q^2}$ .

## B $\bar{B} \rightarrow D^* \tau^- \bar{\nu}_\tau$ details

The  $\bar{B} \rightarrow D^* \tau^- \bar{\nu}_\tau$  differential decay rates for the lepton helicity  $\lambda_\tau = \pm \frac{1}{2}$  are

$$\begin{aligned} \frac{d\Gamma^{D^*}[\lambda_\tau = -1/2]}{dq^2 d \cos \theta_l} &= N |p_{D^*}| \left[ 2|\mathcal{A}_0|^2 \sin^2 \theta_l + (|\mathcal{A}_\parallel|^2 + |\mathcal{A}_\perp|^2)(1 + \cos \theta_l)^2 - 4\text{Re}[\mathcal{A}_\parallel \mathcal{A}_\perp^*] \cos \theta_l \right], \\ \frac{d\Gamma^{D^*}[\lambda_\tau = 1/2]}{dq^2 d \cos \theta_l} &= N |p_{D^*}| \frac{m_\tau^2}{q^2} \left[ 2|\mathcal{A}_0 \cos \theta_l - \mathcal{A}_{tP}|^2 + (|\mathcal{A}_\parallel|^2 + |\mathcal{A}_\perp|^2) \sin^2 \theta_l \right]. \end{aligned} \quad (30)$$

The differential decay rate corresponding to the helicity  $\lambda_\tau = 1/2$  vanishes for the light leptons ( $e, \mu$ ).

The relevant form factors for the  $B \rightarrow D^*$  matrix elements of the vector  $V_\mu = \bar{c}\gamma^\mu b$  and axial-vector  $A_\mu = \bar{c}\gamma^\mu \gamma_5 b$  currents are defined as [22]

$$\begin{aligned} \langle D^*(p_{D^*}, \epsilon^*) | V_\mu | \bar{B}(p_B) \rangle &= \frac{2iV(q^2)}{m_B + m_{D^*}} \varepsilon_{\mu\nu\rho\sigma} \epsilon^{*\nu} p_{D^*}^\rho p_B^\sigma, \\ \langle D^*(p_{D^*}, \epsilon^*) | A_\mu | \bar{B}(p_B) \rangle &= 2m_{D^*} A_0(q^2) \frac{\epsilon^* \cdot q}{q^2} q_\mu + (m_B + m_{D^*}) A_1(q^2) \left[ \epsilon_\mu^* - \frac{\epsilon^* \cdot q}{q^2} q_\mu \right] \\ &\quad - A_2(q^2) \frac{\epsilon^* \cdot q}{(m_B + m_{D^*})} \left[ (p_B + p_{D^*})_\mu - \frac{m_B^2 - m_{D^*}^2}{q^2} q_\mu \right]. \end{aligned} \quad (31)$$

In addition, from Eq. (31) one can show that the  $B \rightarrow D^*$  matrix element for the scalar current vanishes and for the pseudoscalar current reduces to

$$\langle D^*(p_{D^*}, \epsilon^*) | \bar{c} \gamma_5 b | \bar{B}(p_B) \rangle = -\frac{2m_{D^*} A_0(q^2)}{m_b(\mu) + m_c(\mu)} \epsilon^* \cdot q. \quad (32)$$

The expression of the hadronic helicity amplitudes for the  $\bar{B} \rightarrow D^* \tau \bar{\nu}_\tau$  decays are

$$\begin{aligned} \mathcal{A}_0 &= \frac{1}{2m_{D^*} \sqrt{q^2}} \left[ (m_B^2 - m_{D^*}^2 - q^2)(m_B + m_{D^*}) A_1(q^2) - \frac{4m_B^2 |p_{D^*}|^2}{m_B + m_{D^*}} A_2(q^2) \right] (1 - g_A), \\ \mathcal{A}_\pm &= \left[ (m_B + m_{D^*}) A_1(q^2) (1 - g_A) \mp \frac{2m_B V(q^2)}{(m_B + m_{D^*})} |p_{D^*}| (1 + g_V) \right], \\ \mathcal{A}_t &= \frac{2m_B |p_{D^*}| A_0(q^2)}{\sqrt{q^2}} (1 - g_A), \\ \mathcal{A}_P &= -\frac{2m_B |p_{D^*}| A_0(q^2)}{(m_b(\mu) + m_c(\mu))} g_P. \end{aligned} \quad (33)$$

## C $\bar{B} \rightarrow D \tau^- \bar{\nu}_\tau$ results

The  $\bar{B} \rightarrow D \tau \bar{\nu}_\tau$  differential decay rates for the lepton helicity  $\lambda_\tau = \pm \frac{1}{2}$  are

$$\begin{aligned} \frac{d\Gamma^D[\lambda_\tau = -1/2]}{dq^2 d\cos\theta_l} &= 2N |p_D| |H_0|^2 \sin^2 \theta_l, \\ \frac{d\Gamma^D[\lambda_\tau = 1/2]}{dq^2 d\cos\theta_l} &= 2N |p_D| \frac{m_\tau^2}{q^2} |H_0 \cos \theta_l - H_{tS}|^2. \end{aligned} \quad (34)$$

The differential decay rate corresponding to the helicity  $\lambda_\tau = 1/2$  vanishes for the light leptons ( $e, \mu$ ).

The pseudoscalar form factors  $F_+(q^2)$  and  $F_0(q^2)$  of the  $B \rightarrow D$  matrix elements are defined as

$$\begin{aligned} \langle D(p_D) | \bar{c} \gamma^\mu b | \bar{B}(p_B) \rangle &= F_+(q^2) \left[ p_B^\mu + p_D^\mu - \frac{m_B^2 - m_D^2}{q^2} q^\mu \right] + F_0(q^2) \frac{m_B^2 - m_D^2}{q^2} q^\mu, \\ \langle D(p_D) | \bar{c} b | \bar{B}(p_B) \rangle &= \frac{m_B^2 - m_D^2}{m_b(\mu) - m_c(\mu)} F_0(q^2). \end{aligned} \quad (35)$$

The helicity amplitudes are

$$\begin{aligned}
H_0 &= \frac{2m_B|p_D|}{\sqrt{q^2}}F_+(q^2)(1+g_V), \quad H_t = \frac{m_B^2 - m_D^2}{\sqrt{q^2}}F_0(q^2)(1+g_V), \\
H_S &= \frac{m_B^2 - m_D^2}{m_b(\mu) - m_c(\mu)}F_0(q^2)g_S.
\end{aligned} \tag{36}$$

## D Form factors in the Heavy Quark Effective Theory

In the heavy quark limit for the  $b, c$  quarks ( $m_{b,c} \gg \Lambda_{QCD}$ ), both charm and the bottom quark in the hadronic current have to be replaced by static quarks  $h_{v',c}$  and  $h_{v,b}$ , where  $v_B^\mu = p_B/m_B$  and  $v_{D(*)}^\mu = p_{D(*)}/m_{D(*)}$  are the four-velocity of the  $B$  and  $D(D^*)$  mesons, respectively. The  $b \rightarrow c$  transition can be studied in the heavy quark effective theory (HQET). In this effective theory, the matrix elements of the vector and axial vector currents,  $V_\mu$  and  $A_\mu$ , between bottom and charm mesons [23] are defined as

$$\begin{aligned}
\langle D(v') | V_\mu | B(v) \rangle &= \sqrt{m_B m_D} \left[ h_+(w) (v + v')_\mu + h_-(w) (v - v')_\mu \right], \\
\langle D^*(v', \epsilon') | V_\mu | B(v) \rangle &= i\sqrt{m_B m_{D^*}} h_V(w) \epsilon_{\mu\nu\alpha\beta} \epsilon'^{\nu} v'^\alpha v^\beta, \\
\langle D^*(v', \epsilon') | A_\mu | B(v) \rangle &= \sqrt{m_B m_{D^*}} \left[ h_{A1}(w) (w + 1) \epsilon'^*_\mu - h_{A2}(w) \epsilon'^* \cdot v v_\mu \right. \\
&\quad \left. - h_{A3}(w) \epsilon'^* \cdot v v'_\mu \right],
\end{aligned} \tag{37}$$

where the kinematical variable  $w = v_B \cdot v_{D(*)} = (m_B^2 + m_{D(*)}^2 - q^2)/2m_B m_{D(*)}$ .

The form factors  $F_+(q^2)$  and  $F_0(q^2)$  in Eq. (35) are related to the form factors  $h_+(w)$  and  $h_-(w)$  via

$$F_+(q^2) = \frac{V_1(w)}{R_D}, \quad F_0(q^2) = \frac{(1+w)R_D}{2} S_1(w), \tag{38}$$

where

$$\begin{aligned}
V_1(w) &= \left[ h_+(w) - \frac{(1-r)}{(1+r)} h_-(w) \right], \\
S_1(w) &= \left[ h_+(w) - \frac{(1+r)}{(1-r)} \frac{(w-1)}{(w+1)} h_-(w) \right].
\end{aligned} \tag{39}$$

Here  $R_D = 2\sqrt{m_B m_D}/(m_B + m_D)$  and  $r = m_D/m_B$ . We will use the parametrization of the form factor  $V_1(w)$  as given by [17]

$$V_1(w) = V_1(1)[1 - 8\rho_1^2 z + (51\rho_1^2 - 10)z^2 - (252\rho_1^2 - 84)z^3], \tag{40}$$

where  $z = (\sqrt{w+1} - \sqrt{2})/(\sqrt{w+1} + \sqrt{2})$ . The numerical values of the free parameters are [24]

$$\begin{aligned} V_1(1)|V_{cb}| &= (43.0 \pm 1.9 \pm 1.4) \times 10^{-3}, \\ \rho_1^2 &= 1.20 \pm 0.09 \pm 0.04. \end{aligned} \quad (41)$$

For the form factor  $S_1(w)$  we employ the parameterization as in [11],

$$S_1(w) = [1.0036 - 0.0068(w1) + 0.0017(w1)^2]V_1(w). \quad (42)$$

In the HQET, the helicity amplitudes in Eq. (34) becomes

$$\begin{aligned} H_0 &= m_B(1+r)\sqrt{\frac{r(w^2-1)}{(1+r^2-2rw)}}V_1[w](1+g_V), \\ H_{tS} &= \frac{m_B(1-r)\sqrt{r}(w+1)}{\sqrt{(1+r^2-2rw)}}S_1[w]\left[(1+g_V) - \frac{m_B^2(1+r^2-2rw)}{m_l(m_b(\mu)-m_c(\mu))}g_S\right]. \end{aligned} \quad (43)$$

Now we consider the form factors for the  $B \rightarrow D^*$  matrix element in the HQET. The form factors  $h_{A_i}(w)$  are related to the form factors in Eq. (31) [10, 17, 25] in the following way,

$$\begin{aligned} A_1(q^2) &= R_{D^*}\frac{w+1}{2}h_{A_1}(w), \quad A_0(q^2) = \frac{R_0(w)}{R_{D^*}}h_{A_1}(w), \\ A_2(q^2) &= \frac{R_2(w)}{R_{D^*}}h_{A_1}(w), \quad V(q^2) = \frac{R_1(w)}{R_{D^*}}h_{A_1}(w), \end{aligned} \quad (44)$$

where  $R_{D^*} = 2\sqrt{m_B m_D^*}/(m_B + m_D^*)$ . The  $w$  dependence of the form factors can be found in [10, 17] and the summary of the results are

$$\begin{aligned} h_{A_1}(w) &= h_{A_1}(1)\left[1 - 8\rho^2 z + (53\rho^2 - 15)z^2 - (231\rho^2 - 91)z^3\right], \\ R_1(w) &= R_1(1) - 0.12(w-1) + 0.05(w-1)^2, \\ R_2(w) &= R_2(1) + 0.11(w-1) - 0.06(w-1)^2, \\ R_0(w) &= R_0(1) - 0.11(w-1) + 0.01(w-1)^2, \end{aligned} \quad (45)$$

where  $z = (\sqrt{w+1} - \sqrt{2})/(\sqrt{w+1} + \sqrt{2})$ . The numerical values of the free parameters  $\rho^2$ ,  $h_{A_1}(1)$ ,  $R_1(1)$  and  $R_2(1)$  are taken from [25],

$$\begin{aligned} h_{A_1}(1)|V_{cb}| &= (34.6 \pm 0.2 \pm 1.0) \times 10^{-3}, \\ \rho^2 &= 1.214 \pm 0.034 \pm 0.009, \\ R_1(1) &= 1.401 \pm 0.034 \pm 0.018, \\ R_2(1) &= 0.864 \pm 0.024 \pm 0.008, \end{aligned} \quad (46)$$

and  $R_0(1) = 1.14$  is taken from [10]. In the numerical analysis, we allow 10% uncertainties in the  $R_0(1)$  value to account higher order corrections.

In the HQET, the transversity amplitudes of Eq. (33) become

$$\begin{aligned}\mathcal{A}_0 &= \frac{m_B(1-r_*)(w+1)\sqrt{r_*}}{\sqrt{(1+r_*^2-2r_*w)}}h_{A_1}(w)\left[1+\frac{(w-1)(1-R_2(w))}{(1-r_*)}\right](1-g_A), \\ \mathcal{A}_\parallel &= m_B\sqrt{2r_*}(w+1)h_{A_1}(w)(1-g_A), \\ \mathcal{A}_\perp &= -m_B\sqrt{2r_*(w^2-1)}h_{A_1}(w)R_1(w)(1+g_V),\end{aligned}\tag{47}$$

where  $r_* = m_{D^*}/m_B$ .

## References

- [1] K. Ikado *et al.*, Phys. Rev. Lett. **97**, 251802 (2006) [arXiv:hep-ex/0604018].
- [2] See for example, B. Bhattacharjee, A. Dighe, D. Ghosh and S. Raychaudhuri, Phys. Rev. D **83**, 094026 (2011) [arXiv:1012.1052 [hep-ph]].
- [3] A. Filipuzzi, J. Portoles and M. Gonzalez-Alonso, arXiv:1203.2092 [hep-ph].
- [4] U. Nierste, S. Trine and S. Westhoff, Phys. Rev. D **78**, 015006 (2008) [arXiv:0801.4938 [hep-ph]].
- [5] A. Matyja *et al.* [Belle Collaboration], Phys. Rev. Lett. **99**, 191807 (2007) [arXiv:0706.4429 [hep-ex]].
- [6] B. Aubert *et al.* [BABAR Collaboration], Phys. Rev. Lett. **100**, 021801 (2008) [arXiv:0709.1698 [hep-ex]].
- [7] I. Adachi *et al.* [Belle Collaboration], arXiv:0910.4301 [hep-ex].
- [8] A. Bozek *et al.* [Belle Collaboration], Phys. Rev. D **82**, 072005 (2010) [arXiv:1005.2302 [hep-ex]].
- [9] [BaBar Collaboration], arXiv:1205.5442 [hep-ex].
- [10] S. Fajfer, J. F. Kamenik and I. Nisandzic, arXiv:1203.2654 [hep-ph].
- [11] Y. Sakaki and H. Tanaka, arXiv:1205.4908 [hep-ph].
- [12] S. Fajfer, J. F. Kamenik, I. Nisandzic and J. Zupan, arXiv:1206.1872 [hep-ph]; A. Crivellin, C. Greub and A. Kokulu, arXiv:1206.2634 [hep-ph].

- [13] T. Bhattacharya, V. Cirigliano, S. D. Cohen, A. Filipuzzi, M. Gonzalez-Alonso, M. L. Graesser, R. Gupta and H. -W. Lin, Phys. Rev. D **85**, 054512 (2012) [arXiv:1110.6448 [hep-ph]]; C. -H. Chen and C. -Q. Geng, Phys. Rev. D **71**, 077501 (2005) [hep-ph/0503123].
- [14] See for example, A. Rashed, M. Duraisamy and A. Datta, arXiv:1204.2023 [hep-ph]; A. Datta, P. J. O'Donnell, Z. H. Lin, X. Zhang and T. Huang, Phys. Lett. B **483**, 203 (2000) [hep-ph/0001059]. B. Bhattacharjee, S. S. Biswal and D. Ghosh, Phys. Rev. D **83**, 091501 (2011) [arXiv:1102.0545 [hep-ph]].
- [15] See for e.g. A. Datta, Phys. Rev. D **66**, 071702 (2002) [hep-ph/0208016]; A. Datta and P. J. O'Donnell, Phys. Rev. D **72**, 113002 (2005) [hep-ph/0508314]; A. Datta, Phys. Rev. D **74**, 014022 (2006) [hep-ph/0605039]; A. Datta, Phys. Rev. D **78**, 095004 (2008) [arXiv:0807.0795 [hep-ph]]; C. -W. Chiang, A. Datta, M. Duraisamy, D. London, M. Nagashima and A. Szykman, JHEP **1004**, 031 (2010) [arXiv:0910.2929 [hep-ph]].
- [16] M. Neubert, Phys. Rept. **245**, 259 (1994) [hep-ph/9306320].
- [17] I. Caprini, L. Lellouch and M. Neubert, Nucl. Phys. B **530**, 153 (1998) [hep-ph/9712417].
- [18] K. Nakamura *et al.* [Particle Data Group Collaboration], J. Phys. G **37**, 075021 (2010).
- [19] D. Asner *et al.* [Heavy Flavor Averaging Group Collaboration], arXiv:1010.1589 [hep-ex].
- [20] J. G. Korner and G. A. Schuler, Z. Phys. C **46**, 93 (1990).
- [21] A. Kadeer, J. G. Korner and U. Moosbrugger, Eur. Phys. J. C **59**, 27 (2009) [hep-ph/0511019].
- [22] M. Beneke and T. Feldmann, Nucl. Phys. B **592**, 3 (2001) [hep-ph/0008255].
- [23] A. F. Falk and M. Neubert, Phys. Rev. D **47**, 2965 (1993) [hep-ph/9209268].
- [24] B. Aubert *et al.* [BABAR Collaboration], Phys. Rev. Lett. **104**, 011802 (2010) [arXiv:0904.4063 [hep-ex]].
- [25] W. Dungen *et al.* [Belle Collaboration], Phys. Rev. D **82**, 112007 (2010) [arXiv:1010.5620 [hep-ex]].